Engineering 49 (2025) 290–303

Contents lists available at ScienceDirect

Engineering

journal homepage: www.elsevier.com/locate/eng

Research
Medical Engineering—Article

Berberine Protects Cerebral Vessels and Alleviates Diabetic Encephalopathy by Inhibiting the Production of δ-Valerobetaine in the Gut Microbiota

Zheng-Wei Zhang [a,#], Wei-Ping Wang [a,#], Jia-Chun Hu [a,#], Jin-Yue Lu [a,#], Ru Feng [a], Shao-Feng Xu [a], Ling Wang [a], Jie Fu [a], Hang Yu [a], Hui Xu [a], Hao-Jian Zhang [a], Xin-Yu Yang [a], Zhao Zhai [a], Jing-Yue Wang [a], Meng-Liang Ye [a], Heng-Tong Zuo [a], Jian-Ye Song [a], Yi Zhao [a], Xiang Hui [a], Xiao-Liang Wang [a,b,*], Jian-Dong Jiang [a,*], Yan Wang [a,*]

[a] State Key Laboratory of Bioactive Substance and Function of Natural Medicines, Institute of Materia Medica, Chinese Academy of Medical Sciences & Peking Union Medical College, Beijing 100050, China
[b] State Key Laboratory of Druggability Evaluation and Systematic Translational Medicine, Tianjin 300301, China

ARTICLE INFO

Article history:
Received 26 January 2025
Revised 31 March 2025
Accepted 18 April 2025
Available online 30 April 2025

Keywords:
Berberine
Gut microbiota
Inflammation
δ-Valerobetaine
Diabetic encephalopathy

ABSTRACT

Hyperglycemia in individuals with diabetes causes cognitive impairment, called diabetic encephalopathy (DE). The pathogenesis of DE is closely related to angiopathy, and effective treatment is highly desirable. The botanical agent berberine (BBR) effectively lowers blood glucose in diabetic patients. Here, we show for the first time that BBR significantly improved cognitive function in type 2 diabetic encephalopathy KK-Ay (2DEK) mice. High-resolution imaging via fluorescence micro-optical sectioning tomography (fMOST) revealed that the integrity of brain vessels was improved by BBR treatment. The improvements in average vessel diameter, vessel length, and total vessel volume were significant in the parietal association cortex (PtA), as well as in the CA1 and CA3 regions. A mechanistic study revealed that oral BBR inhibited δ-valerobetaine (δ-VB, a metabolite of the gut microbiota) production in the intestine. As intestinal δ-VB can enter the circulation and activate the Toll-like receptor-4 (TLR-4)/myeloid differentiation factor 88 (MyD88)/nuclear factor kappa B (NF-κB) inflammatory pathway in the epithelial cells of blood vessels through interacting with TLR-4, BBR might reduce the intestinal level of δ-VB to protect the cerebral blood vessels of DE mice and improve their brain function. Fecal microbiota transplantation (FMT) using the gut microbiota from BBR-treated mice confirmed the vital role of the gut microbiota. BBR showed a wide range of effects on the gut flora, also increasing short-chain fatty acid (SCFA) production and decreasing lipopolysaccharide (LPS) levels in the intestine by adjusting the abundance of SCFA- or LPS-producing bacteria. The observed therapeutic efficacy *in vivo* revealed a synergistic effect of BBR on the gut microbiota. Conclusively, we found an association between the gut microbiota and blood vessels, of which intestinal δ-VB might be a chemical link. Mainly through downregulating δ-VB in the intestine, BBR protected cerebral vessels and alleviated DE.

1. Introduction

Diabetic encephalopathy (DE) is a form of encephalopathy with abnormal central nervous system function caused by diabetes [1]. The risk of dementia in diabetic patients is approximately 73% greater than that in nondiabetic patients, especially in middle-aged patients with type 2 diabetes (T2D) [2]. DE is closely related to clinical manifestations such as memory loss and learning dysfunction [3], which may lead to serious consequences such as Alzheimer's disease, also called type 3 diabetes [4]. The pathogenesis of DE is very complicated and has not yet been fully elucidated. Among them, factors such as hyperglycemia can cause cerebrovascular inflammation, and the possible mechanism of damage is

* Corresponding authors.
E-mail addresses: wangxl@imm.ac.cn (X.-L. Wang), jiang.jdong@163.com (J.-D. Jiang), wangyan@imm.ac.cn (Y. Wang).
[#] These authors contributed equally to this work.

https://doi.org/10.1016/j.eng.2025.04.018

closely related to the activation of galectin-3 (Gal-3) [5,6], Toll-like receptor-4 (TLR-4) [7], and nuclear factor kappa B (NF-κB) [8,9], among others, leading to compromised cerebral vascular walls, endothelial cell necrosis, and subsequent development of significant pathological injuries, including a reduction in the number of cerebral blood vessels [10]. Therefore, interruption of the inflammatory pathways by targeting TLR-4 and NF-κB might partially restore cerebrovascular physiology and improve brain function.

Research has revealed that the gut microbiota and their metabolites play crucial roles, particularly in the treatment of neurological and psychiatric disorders [11]. Targeting the "gut–brain axis" has become a significant approach in the development of new drugs in recent years. For example, *Morinda officinalis* oligosaccharides can positively modulate the tryptophan→5-hydroxytryptophan→serotonin metabolic pathway through the gut microbiota, thereby promoting the release of 5-hydroxytryptophan and exerting an antidepressant effect [12]. Compounds such as albiflorin or paeoniflorin in Xiaoyao Pills can be metabolized by the gut microbiota and transformed into active metabolites such as benzoic acid [13–15]. These metabolites can cross the blood–brain barrier (BBB), reduce brain fatty acid amide hydrolysis, and exhibit antidepressant effects [15]. Additionally, the metabolites of the gut microbiota may also contribute to the onset and progression of brain diseases. δ-Valerobetaine (δ-VB) is a metabolite of the gut microbiota discovered in recent years, and it can cross the BBB and cause age-related cognitive memory decline and cognitive dysfunction [16]. Studies have shown that δ-VB might directly damage the brain microenvironment, but the detailed mechanism remains unclear. Therefore, modulating the gut microbiota might be a potential strategy for treating DE. Identifying the characteristics of the gut microbiota and their metabolites that might be related to DE has great potential for the discovery of drugs to treat this disease.

Berberine (BBR) is an isoquinoline alkaloid extracted from the traditional Chinese herbal medicine *Coptis chinensis* French. Since 2004, our group, as well as others, has found that BBR is a safe and effective drug in the clinic for the treatment of hyperlipidemia and T2D [17,18]. Unlike most known glucose- or lipid-lowering drugs, BBR administered via the oral route effectively interacts with the gut microbiota [19]. As part of our continuous research [20–25], we showed here that BBR largely improved blood vessels in the brain and alleviated DE through inhibiting δ-VB production in the gut microbiota, thereby interrupting the TLR-4/myeloid differentiation factor 88 (MyD88)/NF-κB inflammatory pathway in vessel endothelial cells. To the best of our knowledge, this is the first report to demonstrate that intestinal δ-VB links the gut microbiota to cerebral vascular inflammation in DE. Currently, it remains difficult to protect brain blood vessels from hyperglycemia-induced inflammation in the clinic, and we consider this discovery highly valuable for potential translation because BBR has been used as an over-the-counter (OTC) drug with good safety records.

2. Materials and methods

2.1. Efficacy of BBR in type 2 diabetic encephalopathy KK-Ay (2DEK) mice

C57BL/6J mice (male, 42–49 days) and KK-Ay mice (male, 42–49 days) were supplied by HFK BIOSCIENCE Co., Ltd. (China). The animals were housed in a controlled environment with free access to food and water. The room temperature was maintained at (22 ± 2) °C with a 12-h light/dark cycle. The research was conducted in accordance with institutional guidelines and ethics and was approved by the Laboratories' Institutional Animal Care and Use Committee of the Chinese Academy of Medical Sciences & Peking Union Medical College (No. 00005020). The research was conducted in accordance with all the ethics guidelines of the Chinese Council on Animal Care.

Thirty KK-Ay mice and ten C57BL/6J mice were adapted for one week before grouping. The C57BL/6J mice were subsequently fed regular fodder (the control group, oral with purified water), and the KK-Ay mice had free access to the KK fodder (No. 1042). The body weight and six-hour fasting blood glucose were measured every week. Fasting blood glucose was measured with an ACCU-CHEK® Performa blood glucose meter (Roche Diabetes Care, Inc., China). After ten weeks, 2DEK mice were selected from among the KK-Ay mice whose six-hour fasting blood glucose level was ≥ 11.1 $mmol \cdot L^{-1}$ for three consecutive weeks. The 2DEK mice were then randomly divided into three groups and given different drugs for ten weeks. The three groups were the model group (oral with purified water, Group M; n = 10), the low-dosage BBR group (oral, 100 $mg \cdot kg^{-1} \cdot d^{-1}$, Group BBR-L; n = 10), and the high-dosage BBR group (oral, 200 $mg \cdot kg^{-1} \cdot d^{-1}$, Group BBR-H; n = 10). BBR was dissolved in purified water. Body weight and the six-hour fasting blood glucose were measured at a fixed time every week during the treatment. At the end of treatment, the oral glucose tolerance test (OGTT) was performed on the mice in each group, with *D*-glucose (2 $g \cdot kg^{-1}$) administered intragastrically, and blood glucose was measured after 15, 30, 60, and 120 min. Then, a novel object recognition test [26] and a step-down test [27] were performed, and fresh feces were collected for 16S ribosomal RNA (rRNA) gene sequencing analysis. According to the results of the step-down test, the mice with the median level in each group were selected for fluorescence micro-optical sectioning tomography (fMOST) [28] (n = 3 for Group M; n = 3 for Group BBR-H). The serum, colons, and brains of other mice were collected. The methods used to determine the other indicators are presented in the supplementary information.

2.2. High-resolution imaging via fMOST

Three KK-Ay mice (from Group M) and three BBR-treated KK-Ay mice (from Group BBR-H) were anesthetized with 10% chloral hydrate solution (0.4 mL per 10 g). Lycopersicon esculentum lectin (LEL) DyLight 488 (140 μL for each mouse) was then injected via the tail vein to label blood vessels. The mice were transcardially perfused with 0.01 $mol \cdot L^{-1}$ phosphate-buffered saline (PBS, pH 7.4) and 4% paraformaldehyde (PFA, w/w). The excised brains were fixed in 4% PFA for 24 h at 4 °C. Furthermore, each brain was rinsed in PBS twice (once every 12 h). Then, the brain was dehydrated in a gradient of ethanol (50% and 75% for 2 h) and dehydrated in absolute ethanol three times (the first two times for 2 h without 0.3% Sudan black B (SBB); the third time overnight with 0.3% SBB). Afterward, each brain was infiltrated using a graded series of LR white resin (50%, 75%, 100% each for 2 h), followed by infiltration with 100% LR white for 48 h. After infiltration, the brain samples were embedded in gelatin capsules and polymerized in a vacuum drying oven with a graded series of temperatures (45 °C for 2 h, 48 °C for 4 h, 50 °C for 2 h). The LR white resin and ethanol used for infiltration and polymerization were combined with 0.3% SBB. The 100% LR white resin was composed of filtrated LR white resin and 2,2′-azobis(2,4-dimethylvaleronitrile) (0.03 g per 5 mL). After the intact brains were removed, stained, and embedded in LR white resin, the samples were subsequently imaged.

Imaging and image preprocessing the resin-embedded intact mouse brains were automatically and continuously sectioned and imaged with the fMOST system (Biomapping 5000; Wuhan OE-Bio Co., Ltd., China). All the image files were saved at an 8-bit depth with a voxel size of 0.35 μm × 0.35 μm × 2 μm. Continuous data acquisition for each mouse brain lasted for four days; the total uncompressed volume of each mouse brain exceeded 3 TB and produced approximately 4500–5000 coronal sections. The raw

imaging dataset of the cerebral vasculature was preprocessed with OE-Bio mapping preprocessing software to assemble mosaics and correct the illumination to improve image quality. The preprocessed dataset was saved in tag image file format (TIFF).

All coronal sections were resampled to a voxel size of 1 μm × 1 μm × 2 μm using the preprocessing software. For convenience in computing the diameter, length, and volume of blood vessels, it was essential to resample high-resolution sections. We converted the resampled sections to Imaris file format (IMS) and used Imaris 9.5 to reconstruct the whole brain. The surface module of Imaris software was applied to build surfaces fit to the blood vessels as much as possible. Considering the differences in brain region volume, the blood vessel surface-to-volume ratio of the brain region was calculated to evaluate the impact of diabetes on mouse cerebral vessels. The single brain subregion was three-dimensionally cropped into a 245 μm × 140 μm × 200 μm cube with an original voxel size of 0.35 μm × 0.35 μm × 2 μm. The selected locations of the brain subregions were as consistent as possible between the KK-Ay mouse group and the BBR-treated mouse group. The filament trace function of Imaris software was used to automatically trace the vascular network. The major quantitative parameters included average blood vessel diameter, vessel length density, and vessel volume. The brain subregion vascular volume and fragment counts were analyzed via the surface function. The filament trace function could have been used to compute the vascular volume, but the filament-measured intravascular volume would be lower than the actual volume.

2.3. Efficacy of fecal microbiota transplantation (FMT) in 2DEK mice

A total of 45 KK-Ay mice (male, 42–49 days) and 15 C57BL/6J mice (male, 42–49 days) were obtained after receiving approval (No. 00005468) and allowed to adapt for one week before grouping. C57BL/6J mice were fed regular fodder (the control group, oral with purified water), and KK-Ay mice had free access to the KK fodder to establish the 2DEK mice. Then, the 2DEK mice were randomly divided into three groups: the model group (oral with purified water, Group M; n = 15), the high-dose BBR group (oral, 200 mg·kg^{-1}·d^{-1}, Group BBR-H; n = 15), and the FMT group (oral with purified water, Group FMT; n = 15). After six weeks of BBR-H treatment, an antibiotic cocktail was used to establish the pseudo-germ-free model, and then FMT was performed using fresh feces from mice in the BBR-H group for three weeks. The antibiotic cocktail preparation and administration protocol was as follows: a mixture containing 10 mg·kg^{-1} each of cefoxitin, gentamicin, metronidazole, and vancomycin was dissolved in PBS. This combination was orally administered to FMT-treated mice for three consecutive days to establish a short-term pseudo-germ-free model, effectively depleting the indigenous gut microbiota. Subsequently, clindamycin hydrochloride (33.3 mg·kg^{-1}) was administered on day 4 to maintain microbiota suppression during the experimental timeline [16]. At the end of treatment, an OGTT was performed. Afterward, the Morris water maze [29], a novel object recognition test, and a step-down test were performed, and fresh feces were collected for 16S rRNA gene sequencing analysis. The serum, colons, and brains of other mice were collected. The methods used to determine the other indicators are presented in the supplementary information.

2.4. Determination of Gal-3 and TLR-4/MyD88/NF-κB signaling in high-glucose-induced bEnd.3 cells

The experiment comprised nine groups, including the control group (only complete medium), Group M (only complete medium), Group lipopolysaccharide (LPS) (100 ng·mL^{-1}), Group δ-VB (200 μmol·L^{-1}), Group sodium acetate (SA) (1 mmol·L^{-1}), Group sodium propionate (SP) (1 mmol·L^{-1}), Group sodium butyrate (SB) (2 mmol·L^{-1}), Group sodium isobutyrate (SIB) (2 mmol·L^{-1}), and Group modified citrus pectin (MCP) (2 mg·mL^{-1}). bEnd.3 cells (Procell Life Science & Technology Co., Ltd., China) in the logarithmic growth phase were plated in six-well plates and cultured for 24 h until the cells filled the wells. Medium with an additional 30 mmol·L^{-1} D-glucose was added to each well, except in the control group, in which an equal amount of complete medium was added. After culturing for 24 h, the compounds mentioned above were added to the respective groups (n = 6). After culturing for 24 h, the bEnd.3 cells were collected and lysed for quantitative determination of the levels of Gal-3, TLR-4, MyD88, NF-κB P65, NF-κB p-P65, tumor necrosis factor-α (TNF-α), interleukin (IL)-1β, and IL-6 by enzyme-linked immunosorbent assay (ELISA) (Beijing Winter Song Boye Biotechnology Co., Ltd., China).

2.5. Statistical analysis

The statistical analysis was performed by the two-tailed Student's t test or one-way analysis of variance (ANOVA) followed by Dunnett's t test using GraphPad Prism version 8 (GraphPad Software, USA). Homogeneity of variance was confirmed using Levene's test prior to ANOVA. Statistical analysis of correlations was performed with Spearman correlation. P values less than 0.05 were considered statistically significant.

The detailed methods and materials are available in the Appendix A.

3. Results

3.1. BBR reduced cerebral vessel damage and protected brain function from hyperglycemia-induced encephalopathy

To determine whether BBR can improve type 2 diabetic encephalopathy, 30 KK-Ay mice were used to construct the 2DEK model (ten C57BL/6J mice were used as the control group). The 2DEK mice were then randomly divided into three groups and given different drugs for ten weeks. The three groups were the model group (Group M; n = 10), the low-dosage BBR group (oral, 100 mg·kg^{-1}·d^{-1}, Group BBR-L; n = 10), and the high-dosage BBR group (oral, 200 mg·kg^{-1}·d^{-1}, Group BBR-H; n = 10) (Fig. S1(a) in Appendix A). At the end of treatment, according to the results of the behavioral test, the mice with the median level in each group were selected for fMOST (n = 3 for Group Model; n = 3 for Group BBR-H). We first examined blood vessels in the brain. To visualize the whole brain vessels with high resolution, we performed a three-dimensional (3D) reconstruction of the vascular network from the imaged sections of both groups. Five hundred sections were projected to a 1000-μm-thick coronal section to reveal 3D images of the brain vessels. In the coronal view, all blood vessels in the entire brain were clearly labeled in red (Fig. 1). The blood vessels in the cortex were particularly abundant, with a greater density than those in other regions, such as the hippocampus and striatum (Fig. 1(a)). When we enlarged the image (with the scale bars was 50 μm or 20 μm), we found that, compared with that of the BBR-H-treated mice, the image background of the KK-Ay model mice was more blurred, with numerous small red dots scattered between blood vessels in the whole brain, including the cortex, hippocampus, and striatum. We then selected the parietal association cortex (PtA), an area rich in blood vessels [30], to observe the notable vascular changes in the KK-Ay mice. The right panel of Fig. 1(a) clearly shows the difference between the untreated KK-Ay model mice (Group M) and the BBR-H-treated KK-Ay mice (Group BBR-H). The integrity of brain capillaries and the permeability of the BBB can be damaged in diabetic mice

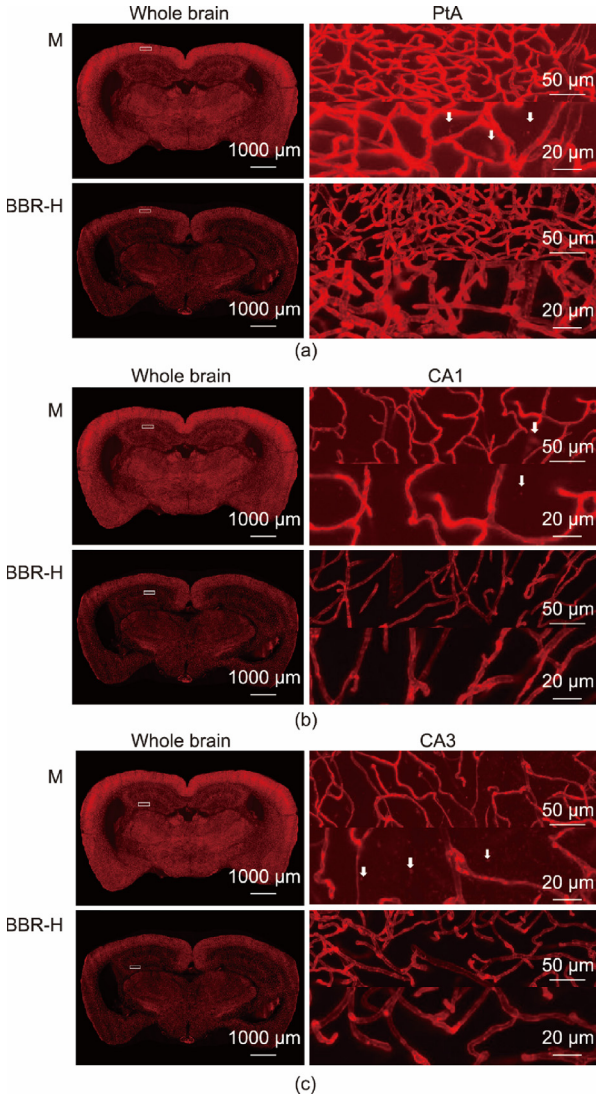

Fig. 1. 3D ultrastructural imaging of cerebral vessels in the 2DEK mice. Typical coronal view of the high-resolution vessel images from whole brain and (a) PtA, (b) CA1, and (c) CA3 before and after BBR-H treatment in KK-Ay mice. The left part of each group is the whole brain vascular imaging and the top-right corner is an enlargement of selected PtA, CA1, and CA3 area (245 μm × 140 μm) indicated as white box in the whole brain, and the bottom-right corner of each group is an enlargement of top-right 1/4 part of selected PtA, CA1, and CA3 area (245 μm × 140 μm).

[31,32]. In the present study, DyLight488 (a red lectin fluorescent dye) was given to the mice to determine its distribution in blood vessels after tail vein injection because the dye only binds to the vascular endothelium and should not appear outside blood vessels. As shown in the right panel of Fig. 1 (PtA, CA1, and CA3), many red fluorescent signals appeared in the tissue between blood vessels, indicating leakage in the brain blood vessels of the untreated KK-Ay model mice and suggesting damage to the endothelial cells of the brain blood vessels. To verify that the permeability of the blood vessels was indeed damaged, we demonstrated that, as shown in Figs. 2(a) and (b), by measuring the grayscale values of the original unprocessed images, the grayscale values of the images from the untreated KK-Ay model mice were markedly greater than those of the BBR-H mice. The results revealed that the image background in the BBR-H group was much clearer than that in the KK-Ay model group, indicating DyLight488 leakage from blood vessels into surrounding tissues in the KK-Ay model mice and a protective effect on blood vessels after BBR treatment. These findings suggest that the integrity of brain vessels is improved by BBR treatment.

To determine how BBR-H improves vascular function, we selected three brain regions, the PtA, CA1, and CA3 regions of the hippocampus, each with a tissue sample size of 245 μm × 140 μm × 200 μm, and measured the changes in vessel diameter, vessel length density, and vessel volume before and after BBR-H administration. As shown in Figs. 2(c)–(e), the average vessel diameter in the PtA and CA1 regions significantly increased by 6.91% and 8.20%, respectively, after BBR-H treatment (n = 3 for each group; $^{*}P < 0.05$, Group BBR-H vs Group M; Figs. 2(c) and (d)), whereas in CA3, the increase was 8.35%, with a P value of 0.10 (Group BBR-H vs Group M; Fig. 2(e)). In the present study, vessel length density refers to the total vessel length in the 245 μm × 140 μm × 200 μm tissue mass, vessel length density is an indicator which was previously reported [33]. BBR-H treatment significantly increased total vessel length density by 25.62% in the PtA region (n = 3 for each group; $^{*}P < 0.05$, Group BBR-H vs Group M; Fig. 2(f)), 9.64% in the CA3 region (P = 0.16; Fig. 2(g)), and had no effect in the CA1 region (Fig. 2(h)). The total vessel volume in the PtA and CA3 regions also significantly increased by 39.80% and 27.73%, respectively, after BBR-H treatment (n = 3 for each group; $^{*}P < 0.05$, $^{**}P < 0.01$, Group BBR-H vs Group M; Figs. 2(i) and (j)); in the CA1 region, the increase was 9.64%, but the difference was not statistically significant (P = 0.42; Fig. 2(k)). Taken together, these findings suggest that BBR-H improved blood vessel function in KK-Ay mice. The improvements in average vessel diameter, vessel length density, and total vessel volume in the PtA were more apparent than those in the CA1 and CA3 regions, which might reflect the rich blood vessel supply in the PtA region [30]. We assumed that the cloudiness of the brain images of the KK-Ay model mice was caused by the hyperglycemia-induced damage to the integrity of blood vessels, which then led to the leakage of fluorescent dye outside the vessels and the labeling of damaged endothelial fragments.

To quantitatively analyze the clarity of the images from the two groups, we compared the grayscale values of the blood vessels in the original unprocessed images; ImageJ software was used to randomly detect the grayscale values of ten data points for blood vessels in each image. The grayscale values of the 100 detected points were then averaged as the grayscale value of the images for each mouse (Fig. 2(a)). The calculated grayscale values of the original images from the KK-Ay model mice and BBR-H-treated mice were (56.32 ± 1.74)% and (29.09 ± 2.21)%, respectively (n = 3; $^{**}P < 0.01$, Group BBR-H vs Group M; Fig. 2(b)). The grayscale value of the images from the KK-Ay model mice was 1.94-fold greater than that of the BBR-H-treated mice. The original brain images of the KK-Ay model mice indeed had a blurry background compared with those of the BBR-H mice, suggesting a protective effect of BBR on the integrity of blood vessels in the brain.

In terms of brain function, all 40 mice recognized similar objects normally (Fig. 3(a)). However, for recognition of new objects, impaired cognitive and memory function in 2DEK mice was restored after oral BBR (100 or 200 mg·kg^{-1}) treatment, as the time spent with new objects significantly increased to 11.50 and 13.70 s in Groups BBR-L and BBR-H, respectively, compared with 10.00 s in Group M ($^{*}P < 0.05$, $^{***}P < 0.001$; Fig. 3(b)). The step-down latency significantly increased to 156.60 and 167.60 s in Groups BBR-L and BBR-H, respectively, compared with 92.10 s in Group M ($^{*}P < 0.05$, $^{**}P < 0.01$; Fig. 3(c)). Additionally, the number of errors significantly decreased from 2.0 to 0.6 or 0.3 in Groups BBR-L and BBR-H compared with Group M ($^{*}P < 0.05$, $^{**}P < 0.01$; Fig. 3(d)).

From a systemic perspective, BBR could also significantly reduce body weight and fasting blood glucose in 2DEK mice in a dose-dependent manner ($^{***}P < 0.001$; Figs. S1(b) and S1(c) in Appendix A), improve their glucose tolerance ($^{***}P < 0.001$;

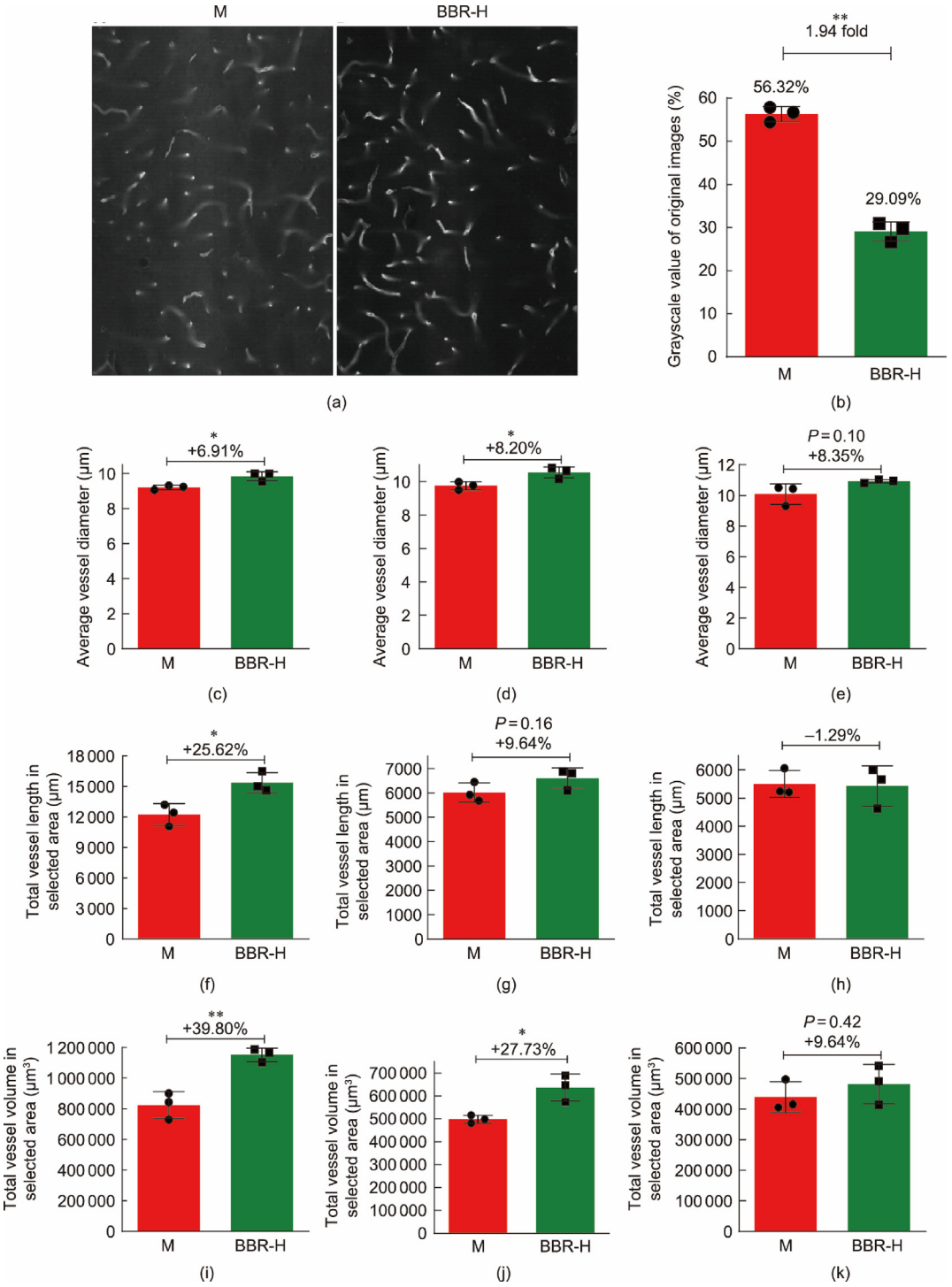

Fig. 2. Evaluation of cerebral vessels in the type 2 DE KK-Ay (2DEK) mice. (a) Comparison of grayscale values of original images between KK-Ay and BBR-H-treated mice. A and B: typical original images from KK-Ay and BBR-H-treated mice, respectively. (b) Statistical histograms of grayscale values for two groups of original images. n = 3, $^{**}P < 0.01$ vs Group M. (c)–(k) Quantitative analysis of three parameters of vascular morphology in three areas in KK-Ay and BBR-H treated mice. Data were analyzed in 262.5 μm × 150 μm × 200 μm tissue volume. (c)–(e) The average vessel diameter in (c) PtA, (d) CA1, and (e) CA3 region before and after BBR-H treatment; (f)–(h) the vessel length density in (f) PtA, (g) CA3, and (h) CA1 region before and after BBR-H treatment; (i)–(k) the total vessel volume in (i) PtA, (j) CA3, and (k) CA1 region before and after BBR-H treatment. n = 3, $^{*}P < 0.05$, $^{**}P < 0.01$ vs Group M.

Figs. S1(d) and (e) in Appendix A), and reduce glycated hemoglobin ($^{**}P < 0.01$, $^{***}P < 0.001$; Fig. S1(f) in Appendix A).

DE is closely related to inflammation [34,35]. Compared with those in the control group, the serum TNF-α, IL-1β, and IL-6 levels in Group M were significantly higher ($^{**}P < 0.01$, $^{***}P < 0.001$). However, the serum levels of TNF-α, IL-1β, and IL-6 of mice treated with BBR were significantly decreased ($^{*}P < 0.05$, $^{**}P < 0.01$, $^{***}P < 0.001$; Figs. S1(g)–(i) in Appendix A), indicating that BBR could ameliorate the high level of inflammation in 2DEK mice. Accordingly, the results from the histological examination revealed that BBR could reduce inflammatory pathological manifestations such as neuronal atrophy in the hippocampus (Fig. 3(e)) and

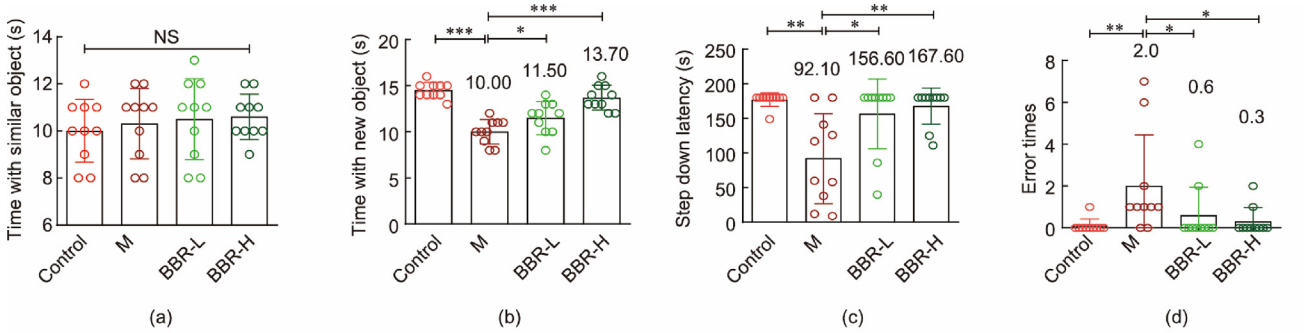
Time with similar object (s)
NS
Control
M
BBR-L
BBR-H
(a)
Time with new object (s)
10.00
11.50
13.70
(b)
Step down latency (s)
92.10
156.60
167.60
(c)
Error times
2.0
0.6
0.3
(d)

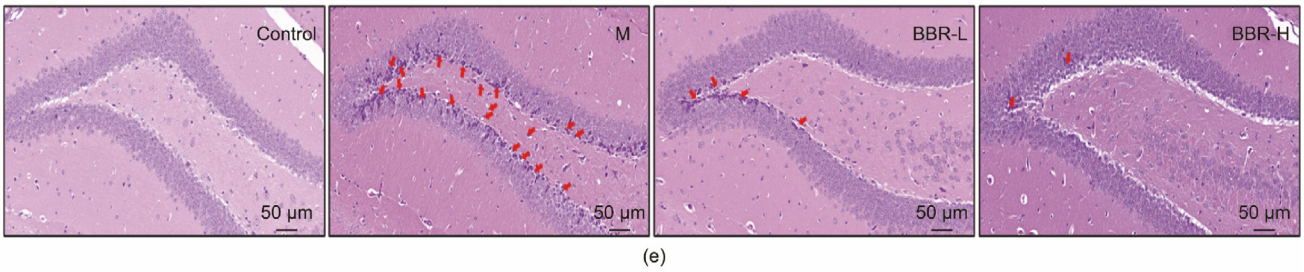
Control
M
BBR-L
BBR-H
50 μm
(e)

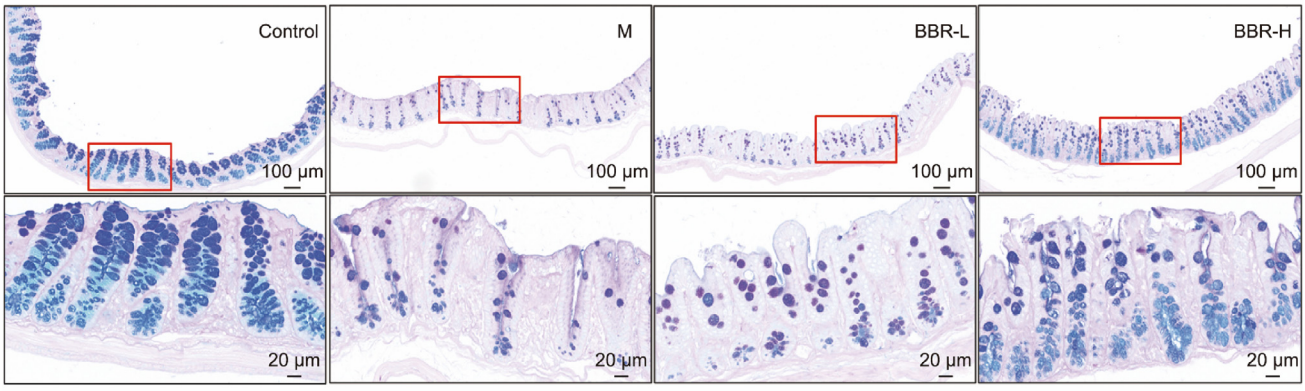
Control
M
BBR-L
BBR-H
100 μm
20 μm
(f)

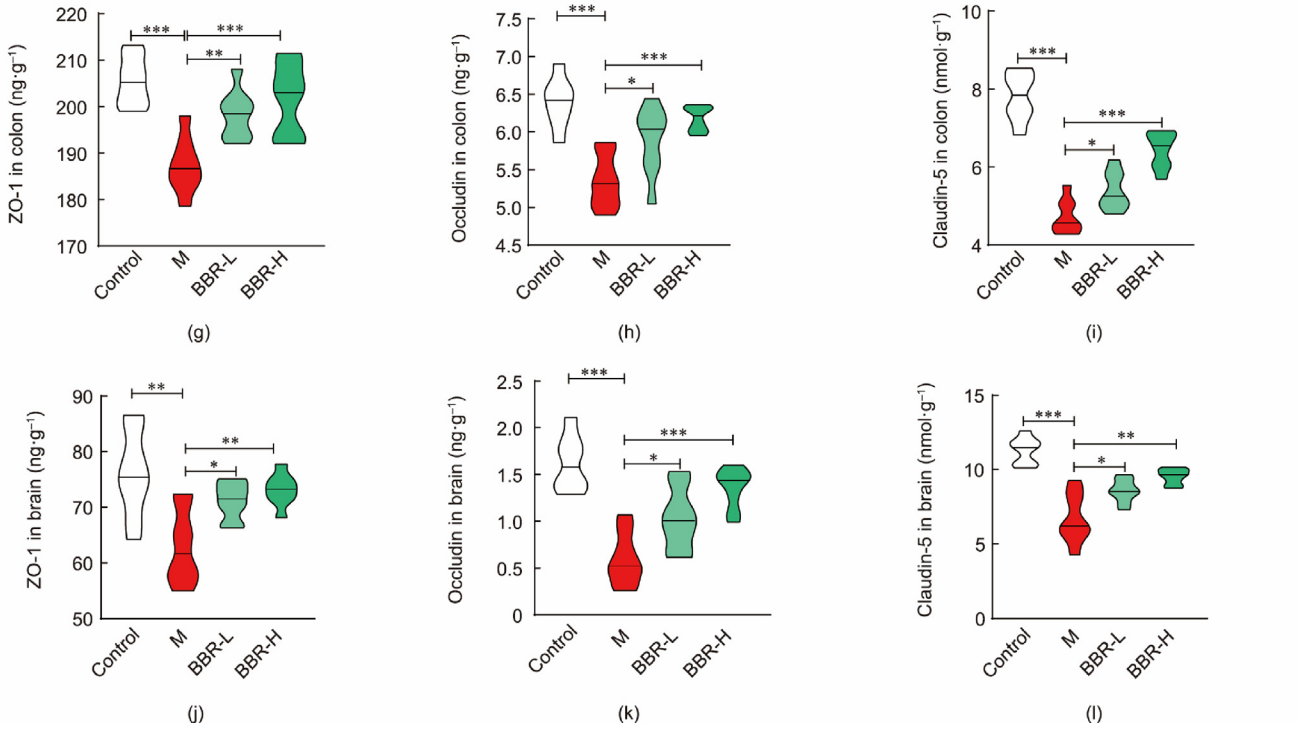
ZO-1 in colon (ng·g⁻¹)
(g)
Occludin in colon (ng·g⁻¹)
(h)
Claudin-5 in colon (nmol·g⁻¹)
(i)
ZO-1 in brain (ng·g⁻¹)
(j)
Occludin in brain (ng·g⁻¹)
(k)
Claudin-5 in brain (nmol·g⁻¹)
(l)

intestinal leakage (Fig. 3(f)) in 2DEK mice and significantly restore the expression of tight junction proteins such as zonula occluden-1 (ZO-1), occludin, and claudin-5 in the epithelial barrier of the colon (*P < 0.05, **P < 0.01, ***P < 0.001; Figs. 3(g)–(i)) and brain (*P < 0.05, **P < 0.01, ***P < 0.001; Figs. 3(j)–(l)). In addition, Gal-3 was examined as it is an inflammation-related protein that could accelerate inflammation and insulin resistance and thus participate in the occurrence and development of diabetes [36]. In this study, we showed that, compared with those in the control group, Gal-3 levels in the colon and brain were greater in Group M (Figs. 4(a) and (b)); however, BBR treatment significantly reduced the expression of Gal-3 in the colon, serum, and brain of mice in the 2DEK group (*P < 0.05, **P < 0.01, ***P < 0.001; Figs. 4(c)–(e)). BBR alleviated inflammatory damage in the colon and hippocampal regions through either local restoration of impaired BBB and intestinal barrier function in 2DEK mice or systematic decreases in inflammatory factors.

These inflammatory markers, including Gal-3 in the brain, serum, and colon, as well as TNF-α, IL-1β, and IL-6 in the serum, were negatively correlated with the behavioral results (*P < 0.05), with correlation coefficients ranging from −0.4867 to −0.6069 in the new object recognition test and from −0.2639 to −0.6914 in the step-down test (Table S1 in Appendix A). Among the inflammatory factors, Gal-3 in the brain might be the one most indicative of the progression of DE, as the largest correlation coefficients of −0.6069 or −0.6914 were observed for Gal-3 in the recognition tests (Table S1), suggesting more severe memory damage with higher levels of Gal-3 in the brain. BBR could reduce Gal-3 in the brain through, at least in part, lowering Gal-3 in the colon in a dose-dependent manner and then alleviate memory impairment.

3.2. BBR relieved DE through its effects on the gut microbiota

As a large amount of BBR accumulates in the intestine after oral administration [37], FMT was used to explore the mode of action of BBR (Fig. S2(a) in Appendix A). To meet the prerequisites for FMT treatment, an antibiotic cocktail was used to remove 87.3% of aerobic bacteria (***P < 0.001; Figs. S2(b) and (c) in Appendix A) and 93.86% of anaerobic bacteria (***P < 0.001; Figs. S2(d) and (e) in Appendix A) in feces. Subsequently, BBR-H was used to treat 2DEK mice as donors for FMT, and the fecal samples were washed with PBS via centrifugation prior to transplantation. In terms of brain function, FMT significantly restored cognitive function impaired by high levels of blood glucose in 2DEK mice (Figs. 4(f) and (g)), as the time spent with the new object significantly increased to 12.60 and 12.50 s in Groups BBR-H and FMT, respectively, with respect to 9.92 s in Group M (*P < 0.05, ***P < 0.001). FMT also significantly restored the impaired memory function in the 2DEK mice (Figs. 4(h) and (i)), as indicated by the step-down latency significantly increasing to 164.46 and 159.29 s in Groups BBR-H and FMT, respectively, with respect to 91.54 s in Group M (*P < 0.05, **P < 0.01). Moreover, the number of errors significantly decreased from 2.31 in Group M to 0.46 and 0.50 in Groups BBR-H and FMT, respectively (*P < 0.05, ***P < 0.001). In addition, BBR-H and FMT further restored the impaired spatial memory in 2DEK mice, indicating that the escape latency was significantly decreased in Groups BBR-H and FMT on the 5th day of training compared with that in Group M (*P < 0.05, ***P < 0.001; Fig. 4(j)). Compared with that in Group M, the first crossing time was significantly decreased to 31.82 or 37.44 s in Group BBR-H and FMT, respectively, compared with 72.34 s in Group M (*P < 0.05, **P < 0.01, ***P < 0.001; Fig. 4(k)). Additionally, the number of crossings was significantly increased from 0.54 in Group M to 2.62 and 2.50 in Groups BBR-H and FMT, respectively (*P < 0.05, **P < 0.01, ***P < 0.001; Fig. 4(l)). These results suggest that the improvement in brain function caused by BBR in mice with DE might result from the gut microbiota.

Furthermore, FMT significantly reduced body weight (***P < 0.001; Fig. S2(f) in Appendix A), fasting blood glucose levels (***P < 0.001; Fig. S2(g) in Appendix A), and glycosylated hemoglobin levels (***P < 0.001; Fig. S2(h) in Appendix A), and improved glucose tolerance in 2DEK mice (***P < 0.001; Figs. S3(a) and (b) in Appendix A). In combination with Group M, FMT also significantly inhibited inflammation in 2DEK mice, as indicated by reduced levels of TNF-α, IL-1β, and IL-6 (*P < 0.05, **P < 0.01, ***P < 0.001; Figs. S3(c)–(e) in Appendix A). Moreover, FMT significantly decreased Gal-3 levels in the brain, serum, and colon (*P < 0.05, **P < 0.01; Figs. S3(f)–(h) in Appendix A) and suppressed Gal-3 expression in the colon and brain (Figs. S3(i) and (j) in Appendix A). Owing to the significant recovery of the expression of tight junction proteins (ZO-1, occludin, and claudin-5) in the colon (*P < 0.05, **P < 0.01; Figs. S4(a)–(c) in Appendix A) and the brain (*P < 0.05, **P < 0.01; Figs. S4(d)–(f) in Appendix A), intestinal leakage caused by inflammatory damage (Fig. S4(g) in Appendix A) and neuronal atrophy of the hippocampus (Fig. S4(h) in Appendix A) were reduced in the 2DEK mice.

3.3. BBR ameliorated DE by regulating the production of the gut microbiota metabolites δ-VB, short-chain fatty acids (SCFAs), and LPS

By analyzing the results from 16S rRNA gene sequencing, we found that BBR could significantly change the diversity and richness of the gut microbiota in 2DEK model mice (Figs. S5(a)–(d) in Appendix A). Moreover, the composition of the gut microbiota differed after BBR treatment (Figs. S5(e) and (f) in Appendix A). At the phylum level, BBR increased the proportion of Bacteroidota and inhibited the excessive growth of Proteobacteria (Fig. 5(a)), which was consistent with the trend of the corresponding order and family level (Figs. 5(b) and (c)). At the genus level, 13 genera, marked with red arrows in Fig. 5(d), such as *Bacteroides*, *Allobaculum*, and *Akkermansia*, were more abundant after BBR treatment, and these genera are closely related to the synthesis of SCFAs [38,39]. Moreover, the other seven genera, marked with blue arrows, especially *Escherichia-Shigella*, *Klebsiella*, and *Citrobacter*, were less abundant (Fig. 5(d)); these genera are closely related to the production of LPS [40].

Similarly, FMT also significantly changed the diversity and richness of the gut microbiota in the 2DEK model mice (Figs. S5(g)–(l)

Fig. 3. BBR improved the brain function and reduced inflammation damage in hippocampus and intestinal leakage of 2DEK mice. (a) Time with similar object in new object recognition (NOR) test after BBR treatment (n = 10). (b) Time with new object in NOR test after BBR treatment (n = 10). (c) Step-down latency in step-down test after BBR treatment (n = 10). (d) Error times in step-down test after BBR treatment (n = 10). (e) Representative images of hematoxylin and eosin (H&E) staining in brain after BBR treatment (scale: 50 μm; the red arrows indicated the pathological manifestations such as neuronal atrophy in the hippocampus). (f) Representative images of AB-PAS staining in colon after BBR treatment (scale: 100 μm, top) and their local enlarged images (scale: 20 μm, bottom). (g) ZO-1 in colon after BBR treatment (n = 8). (h) Occludin in colon after BBR treatment (n = 8). (i) Claudin-5 in colon after BBR treatment (n = 8). (j) ZO-1 in brain after BBR treatment (n = 8). (k) Occludin in brain after BBR treatment (n = 8). (l) Claudin-5 in brain after BBR treatment (n = 8). Error bars represent SEM. Statistical analysis was performed with one-way ANOVA followed by Dunnett-t test (*P < 0.05, **P < 0.01, ***P < 0.001). NS: no significance; SEM: standard errors of the mean.

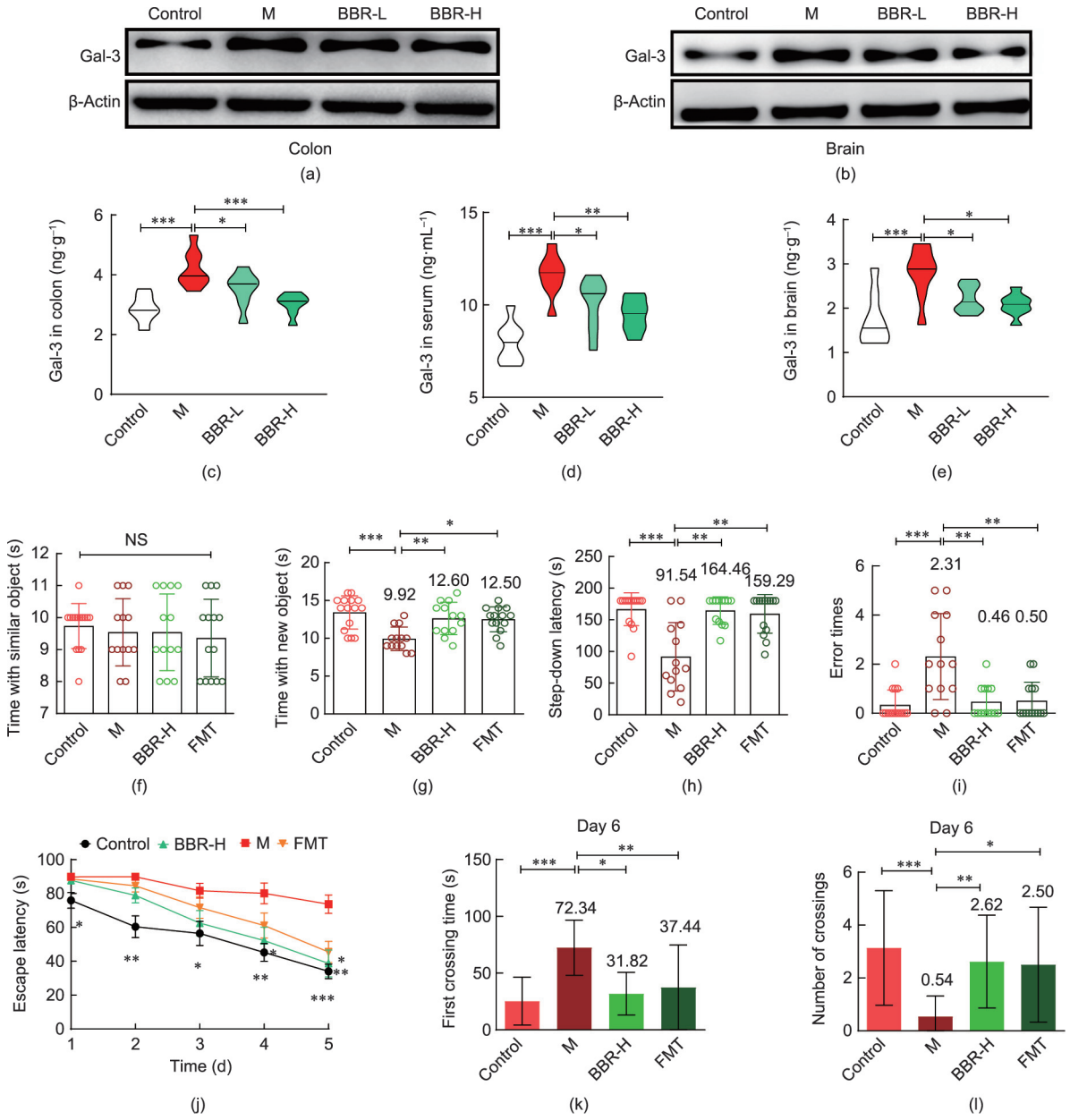

Fig. 4. BBR increased tight junction proteins in brain while reducing Gal-3 in 2DEK mice and FMT improved the brain function of 2DEK mice. (a) Representative western blot images of Gal-3 in colon after BBR treatment. (b) Representative western blot images of Gal-3 in brain after BBR treatment. (c) Gal-3 in colon after BBR treatment (n = 8). (d) Gal-3 in serum after BBR treatment (n = 8). (e) Gal-3 in brain after BBR treatment (n = 8). (f) Time with similar object in NOR test after BBR/FMT treatment (n = 13–15). (g) Time with new object in NOR test after BBR/FMT treatment (n = 13–15). (h) Step-down latency in step-down test after BBR/FMT treatment (n = 13–15). (i) Error times in step-down test after BBR/FMT treatment (n = 13–15). (j) Escape latency in pretraining of Morris water maze after BBR/FMT treatment (n = 13–15). (k) First crossing time in probe trial of Morris water maze after BBR/FMT treatment (n = 13–15). (l) Number of crossings in probe trial of Morris water maze after BBR/FMT treatment (n = 13–15). Statistical analysis was performed with one-way ANOVA followed by Dunnett-t test (*P < 0.05, **P < 0.01, ***P < 0.001).

in Appendix A). Moreover, the composition of the gut microbiota in the FMT group was consistent with that in the BBR-H group (Figs. S5(a)–(f)). FMT promoted the restoration of beneficial bacterial genera, such as *Bacteroides*, *Allobaculum*, and *Akkermansia*, but inhibited the excessive growth of several harmful bacterial genera, such as *Escherichia-Shigella*, *Klebsiella*, and *Citrobacter* (Fig. 6).

Interestingly, both BBR and FMT significantly inhibited the production of δ-VB (*P < 0.05, **P < 0.01, ***P < 0.001; Figs. 7(a)–(f)), a metabolite of the gut microbiota that has been reported to cause cognitive decline [16]. The level of δ-VB was negatively correlated with the results of the new object recognition (NOR) test (time with a new object) and step-down test (step-down latency). The correlation coefficient between δ-VB and NOR test result was −0.4629 in feces, −0.4395 in serum, and −0.5888 in the brain, and the correlation coefficient between δ-VB and the step-down latency was −0.5301 in feces, −0.5239 in serum, and −0.7354 in the brain (Table S2 in Appendix A). Therefore, the δ-VB level in the brain could also be a potential biomarker for the therapeutic effect of BBR on DE, and its level was most strongly correlated with the abundance of *Allobaculum* and *Bilophila*, with a correlation coefficient of −0.7136 and 0.7160, respectively (Table S3 in Appendix A).

In addition, SCFAs were analyzed *in vivo* via gas chromatography–mass spectrometry. The results revealed that BBR significantly increased the levels of acetic acid (AA), propionic acid (PA), butyric acid (BA), and isobutyric acid (IBA) in the feces of

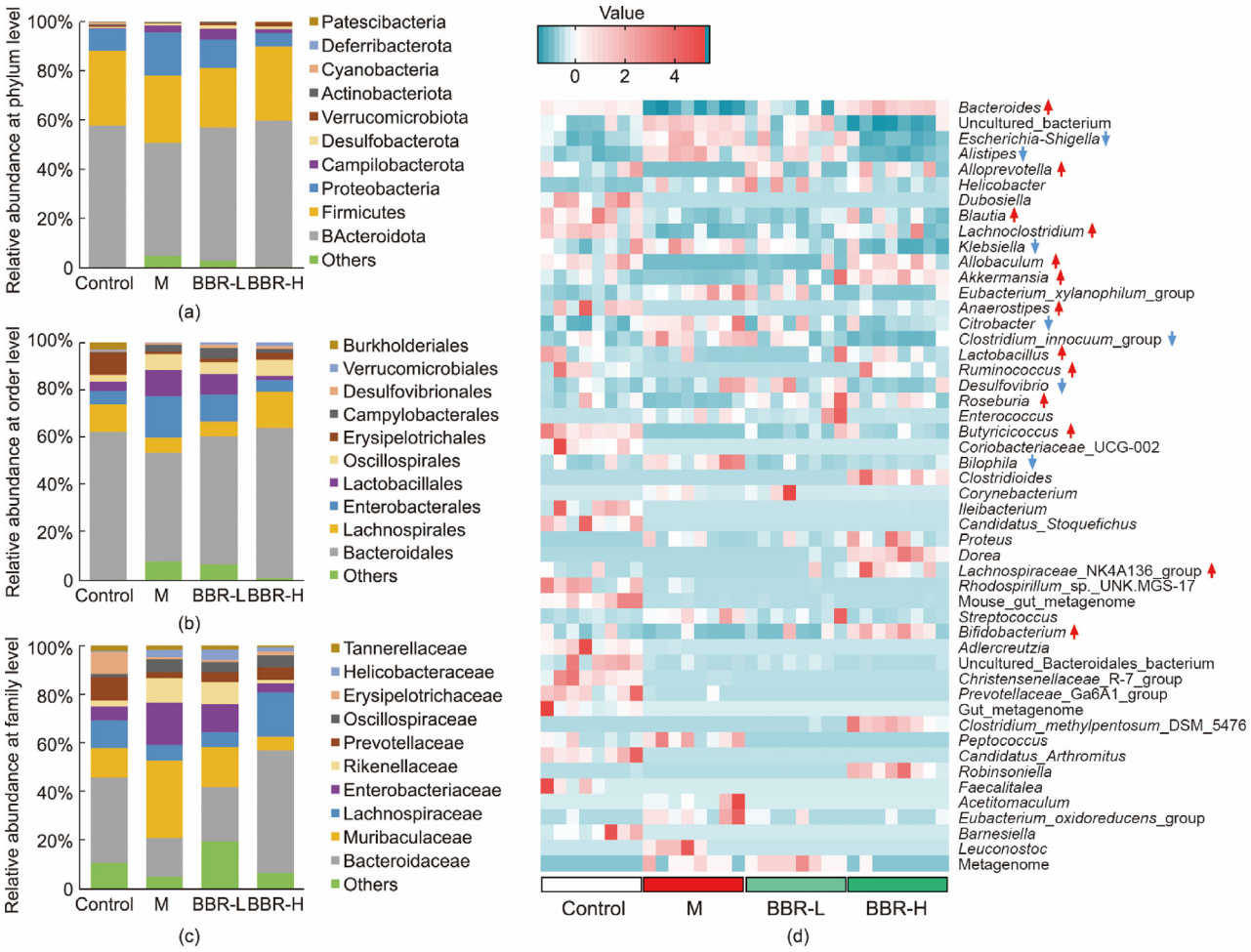

Fig. 5. BBR changed the composition and proportion of gut microbiota from 2DEK. (a) The phylum proportion of gut microbiota in feces after BBR treatment (n = 8). (b) The order proportion of gut microbiota in feces after BBR treatment (n = 8). (c) The family proportion of gut microbiota in feces after BBR treatment (n = 8). (d) The genus proportion of gut microbiota in feces after BBR treatment (n = 8, 13 genera marked with red arrows were significantly up-regulated and seven genera marked with blue arrows were significantly down-regulated after BBR treatment).

2DEK mice (*P < 0.05, **P < 0.01, ***P < 0.001; Figs. S6(a)–(d) in Appendix A). The trends in SCFA levels in the serum and brain were consistent with those in the feces (*P < 0.05, **P < 0.01, ***P < 0.001; Figs. S6(e)–(l) in Appendix A). However, the levels of other SCFAs *in vivo* were not significantly increased after BBR treatment (Fig. S7 in Appendix A). Similarly, FMT also significantly increased AA, PA, and BA levels in 2DEK mice (*P < 0.05, **P < 0.01, ***P < 0.001) and upregulated IBA expression to a certain extent (Fig. S8 in Appendix A). Among them, AA, PA, and BA in fecal samples could be potential pharmacodynamic biomarkers for the effects of BBR on improving the behavioral symptoms of 2DEK mice, with good coefficients of correlation (Table S4 in Appendix A), mainly with *Alloprevotella*, *Butyricicoccus*, and *Allobaculum* (Table S5 in Appendix A).

In contrast, both BBR and FMT significantly reduced the levels of LPS and lipopolysaccharide-binding protein (LBP) in the serum of 2DEK mice (*P < 0.05, **P < 0.01, ***P < 0.001), which is in agreement with the changes in the brain (*P < 0.05, **P < 0.01, ***P < 0.001; Fig. S9 in Appendix A). Thus, a reduction in LPS and LBP in the serum might also be important to BBR in ameliorating DE (Table S6 in Appendix A), particularly regarding its action on LPS- or LBP-producing bacteria such as *Escherichia-Shigella* and *Citrobacter* (Table S7 in Appendix A).

3.4. δ-VB of the gut microbiota regulated the TLR-4/MyD88/NF-κB pathway in the brain microvasculature

Given that the gut flora-derived metabolite δ-VB could be a key molecule associated with DE, we investigated whether and how δ-VB affects the TLR-4/MyD88/NF-κB inflammatory pathway. Thus, molecular docking simulations between δ-VB and TLR-4 were performed first. The results showed that δ-VB could steadily form firm molecular bonds (Table S8 in Appendix A) with all the binding sites of TLR-4, especially the third site (Fig. S10 in Appendix A). Furthermore, the activation of the TLR-4/MyD88/NF-κB pathway and the subsequent production of TNF-α, IL-1β, and IL-6 were inhibited (*P < 0.05, **P < 0.01, *** P< 0.001; Figs. 7(g)–(l)) by a selective inhibitor of TLR-4, TAK-242 [41], in high-glucose-induced cerebral microvascular endothelial (bEnd.3) cells in the presence of δ-VB. These results suggested that δ-VB could activate the TLR-4/MyD88/NF-κB inflammatory pathway through direct binding to TLR-4.

In addition, we found that Gal-3, the inflammatory marker of DE, as mentioned above, was significantly negatively correlated with AA, PA, BA, and IBA levels in feces and was positively correlated with LPS in the brain and δ-VB *in vivo* (*P < 0.05, **P < 0.01, ***P < 0.001; Fig. 8(a)). Moreover, SA, SP, SB, and MCP (a specific

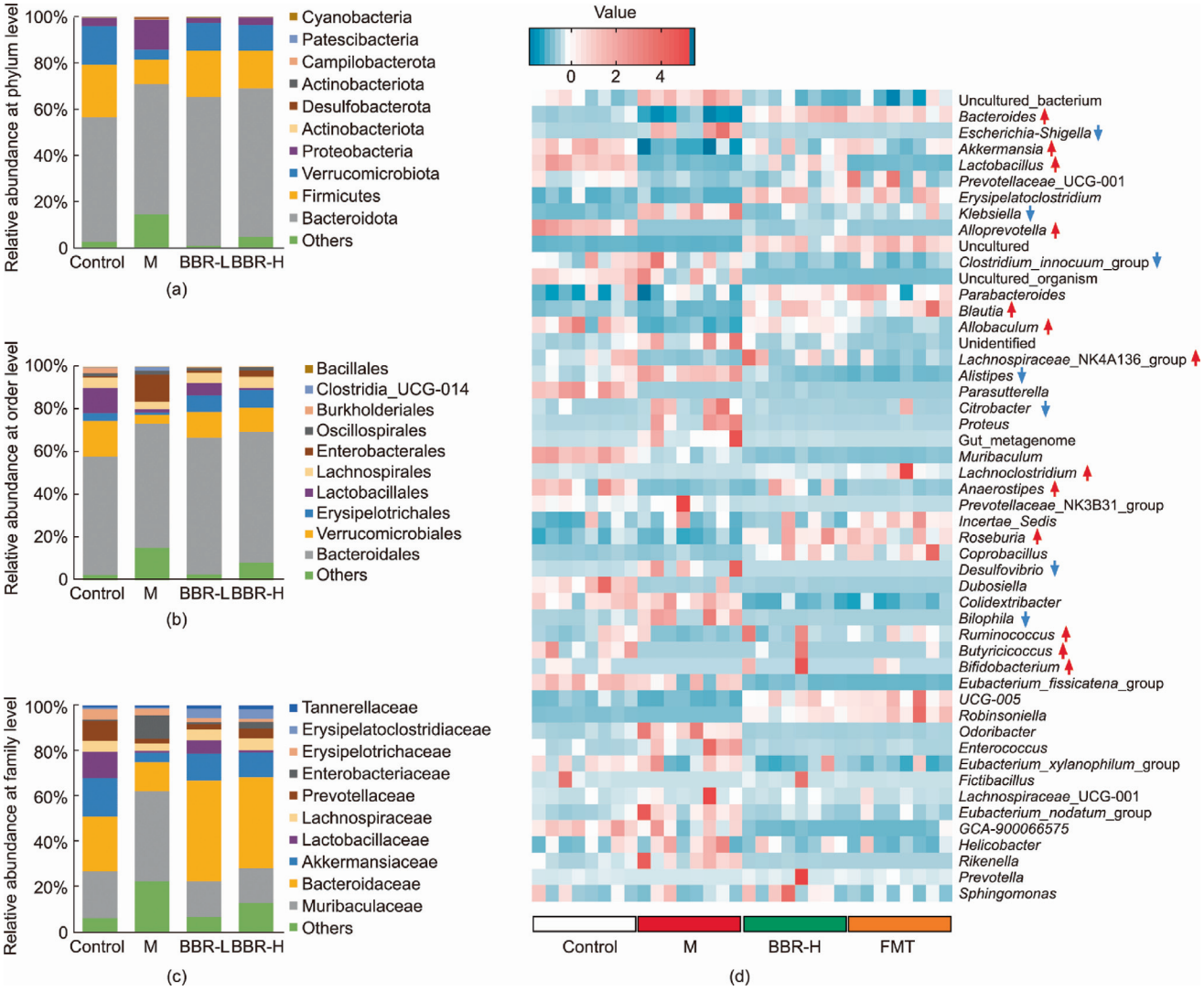

Fig. 6. FMT changed the composition and proportion of gut microbiota from 2DEK. (a) The phylum proportion of gut microbiota in feces after FMT treatment (n = 8). (b) The order proportion of gut microbiota in feces after FMT treatment (n = 8). (c) The family proportion of gut microbiota in feces after FMT treatment (n = 8). (d) The genus proportion of gut microbiota in feces after FMT treatment (n = 8, 13 genera marked with red arrows were significantly up-regulated and seven genera marked with blue arrows were significantly down-regulated after FMT treatment).

inhibitor of Gal-3) inhibited the production of Gal-3 in high-glucose-treated bEnd.3 cells ($^{*}P < 0.05$, $^{**}P < 0.01$, $^{***}P < 0.001$; Fig. 8(b)), accompanied by inhibition of the activation of the TLR-4/MyD88/NF-κB pathway ($^{*}P < 0.05$, $^{**}P < 0.01$, $^{***}P < 0.001$; Figs. 8(c)–(e)) and the production of TNF-α, IL-1β, and IL-6 ($^{*}P < 0.05$, $^{**}P < 0.01$, $^{***}P < 0.001$; Figs. 8(f)–(h)). In contrast, LPS and δ-VB further aggravated the activation of this inflammatory pathway ($^{*}P < 0.05$; Fig. 8(b)), followed by increased production of TNF-α ($^{*}P < 0.05$), IL-1β ($^{*}P < 0.05$), and IL-6 (Figs. 8(f)–(h)).

4. Discussion

The pathogenesis of secondary diseases in T2D is often associated with hyperglycemia-induced chronic inflammation in the blood vessels of diseased organs, and DE is an example in the brain [42]. In the present study, we discovered that the homeostasis of the gut microbiota appears to be associated with the status of blood vessels, at least in the brain. In addition, intestinal δ-VB might be the chemical link between the gut and blood vessels, as it can enter the blood, activate the TLR-4/MyD88/NF-κB pathway and then cause blood vessel inflammation in the brain. Oral BBR downregulated δ-VB production in the gut microbiota and inhibited the TLR-4/MyD88/NF-κB inflammatory pathway in brain microvessels, thereby ameliorating DE. As T2D is a systemic disease, optimal drug treatment for its secondary diseases, such as DE, should include ① reducing blood glucose and ② suppressing inflammation in blood vessels. We consider BBR, which has been successfully used to lower blood glucose in patients, to be an ideal agent for treating DE [18].

The most notable discovery in this study is the remarkable improvement in the microvessel structure and volume by BBR in the DE brain, and to our knowledge, such a substantial beneficial effect on blood vessels by therapeutic agents has not been reported before. This cerebral vessel examination in 2DEK mice was performed using a new technology combining 3D ultrastructural imaging (3DUI) with fMOST (Fig. 1). Notably, the fMOST system, a novel neuro-optical imaging system, also has great advantages in the reconstruction and quantitative analysis of cerebral vessels with a resolution as high as a 1-μm voxel [43]. Thus, the methods and techniques used for blood vessel analysis are considered to be cutting-edge and precise methods for drawing conclusions. With these new methods, we found that BBR improved cerebral vessel parameters overall, including diameter, length, density, and total

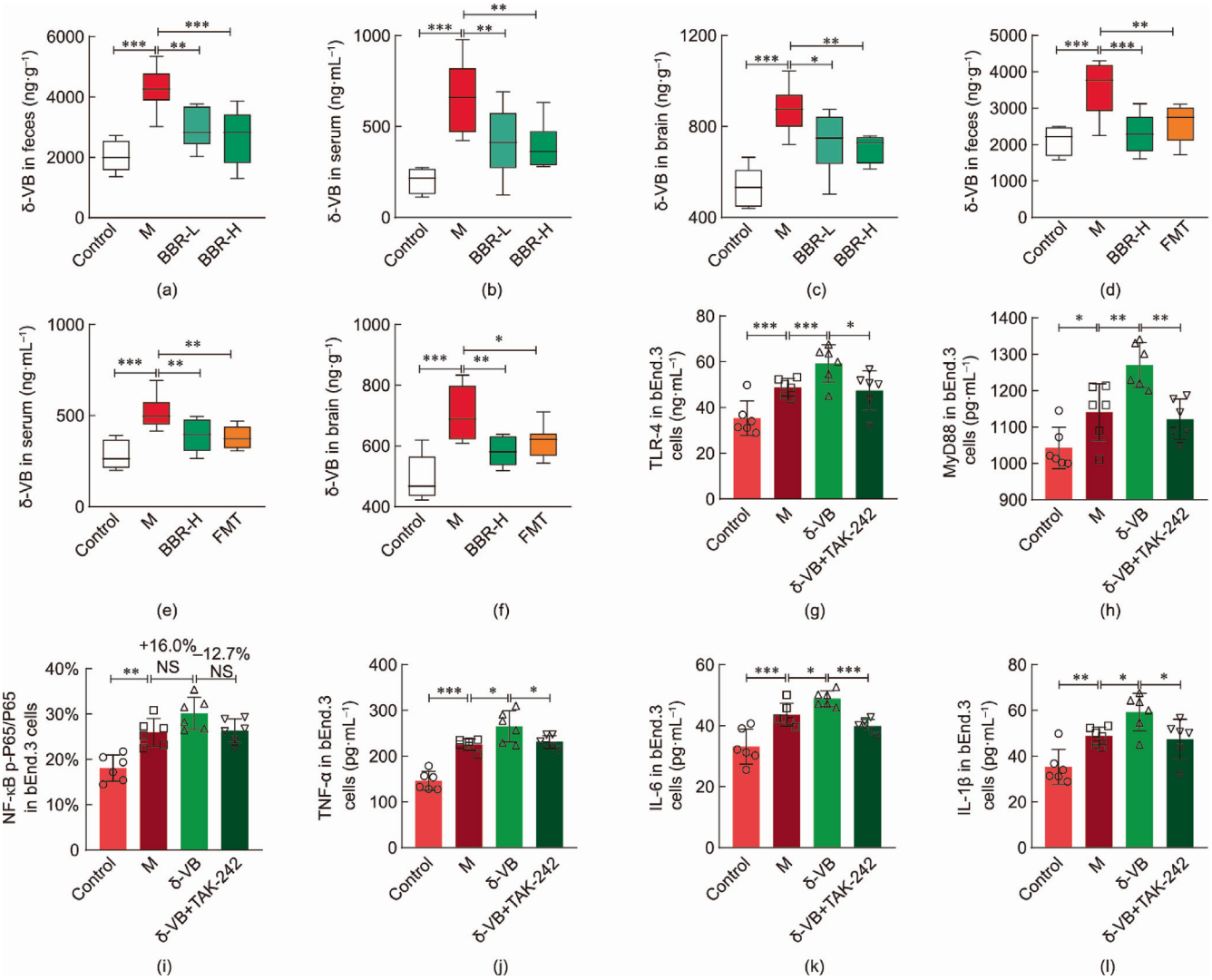

Fig. 7. BBR regulates the production of δ-VB in 2DEK mice, thereby mediating the mechanism of action of the TLR-4/MyD88/NF-κB pathway in high glucose-induced bEnd.3 cells. (a) δ-VB in feces after BBR treatment (n = 8). (b) δ-VB in serum after BBR treatment (n = 8). (c) δ-VB in brain after BBR treatment (n = 8). (d) δ-VB in feces after BBR/FMT treatment (n = 8). (e) δ-VB in serum after BBR/FMT treatment (n = 8). (f) δ-VB in brain after BBR/FMT treatment (n = 8). (g) TLR-4 in bEnd.3 cells with or without the inhibitor (n = 6). (h) MyD88 in bEnd.3 cells with or without the inhibitor (n = 6). (i) p-P65/P65 of NF-κB in bEnd.3 cells with or without the inhibitor (n = 6). (j) TNF-α in bEnd.3 cells with or without the inhibitor (n = 6). (k) IL-6 in bEnd.3 cells with or without the inhibitor (n = 6). (l) IL-1β in bEnd.3 cells with or without the inhibitor (n = 6). Statistical analysis was performed with one-way ANOVA followed by Dunnett-t test (*P < 0.05, **P < 0.01, ***P < 0.001).

volume (Figs. 2(c)–(k)), in addition to the effect of BBR on the endothelial integrity of blood vessels. These findings suggest that BBR is a potential agent for DE therapy that works through a group of actions favorable for cerebral vessel health.

Interestingly, these actions were associated with the gut microbiota, suggesting a gut–vessel axis. The metabolite δ-VB might be a chemical link between the gut flora and blood vessels, as δ-VB activates the TLR-4/MyD88/NF-κB pathway in blood vessel endothelial cells. δ-VB is a functional metabolite derived from the gut microbiota that enters the circulation and exists in organs such as the brain. Excessive levels of δ-VB cause cardiac hypertrophy [44] and brain function decline [16], but the pathogenic mechanism of δ-VB remains unclear. We found that a high level of δ-VB in the brain seemed to be associated with behavioral symptoms in 2DEK mice and that activation of the TLR-4/MyD88/NF-κB pathway in the epithelium might be at least part of the mechanism involved. In fact, no clinical agent has been found to be effective in lowering δ-VB in humans. If further clinical studies verify that BBR could improve cognition and memory in DE by downregulating δ-VB in the gut microbiota, it could facilitate rational drug design against DE in the future. In addition, as the TLR-4 ligand TAK-242 effectively inhibited the activation of the TLR-4/MyD88/NF-κB pathway, we assume that the interaction between TLR-4 and δ-VB is a potential drug target for DE.

Studies have shown that the oral administration of BBR substantially regulates the gut microbiota in the host, which subsequently contributes to the effects of BBR in treating diseases [23–25,45]. For example, BBR increases levodopa production in the gut microbiota to improve Parkinson's disease; moreover, it reduces trimethylamine N-oxide (TMAO) and p-cresol formation in the intestine and thus ameliorates atherosclerosis and chronic kidney disease [23–25]. This is the first report to show the downregulatory effect of BBR on δ-VB production in the gut microbiota, and the results were verified using the BBR-free FMT from BBR-treated mice. In general, we consider it important to understand the mechanism by which BBR protects blood vessels. In addition, the roles of the microbiota are broad and may involve substances other than the metabolites discovered in this study. However, our research revealed that BBR significantly changed the composition of the gut microbiota in 2DEK mice, in which the SCFA-producing genera increased and the

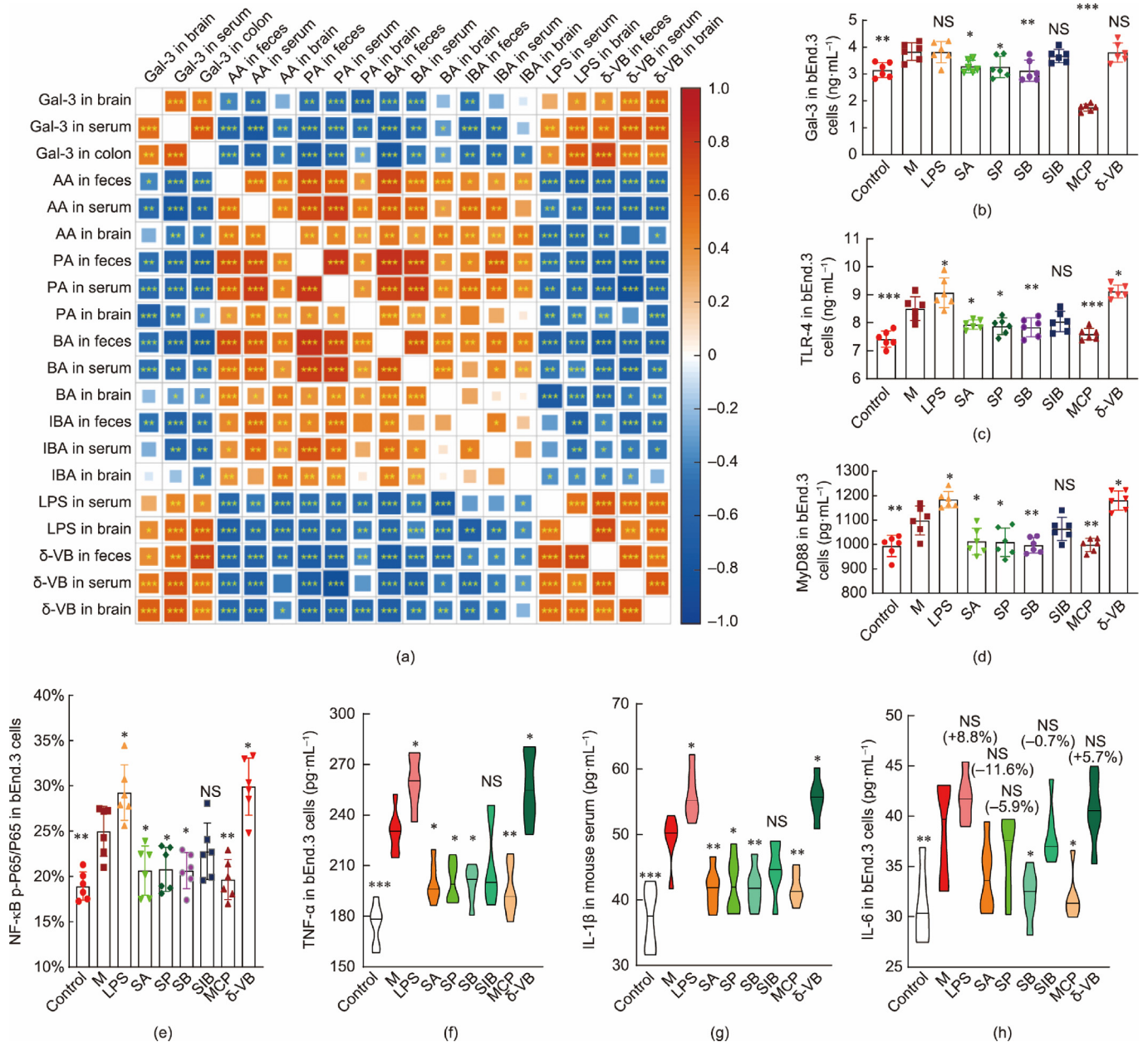

Fig. 8. The mechanism of δ-VB/SCFAs/LPS on TLR-4/MyD88/NF-κB pathway in high glucose-induced bEnd.3 cells. (a) Correlation analysis between δ-VB/SCFAs/LPS and Gal-3 *in vivo* after BBR treatment. (b) Gal-3 in bEnd.3 cells after treatment (n = 6). (c) TLR-4 in bEnd.3 cells after treatment (n = 6). (d) MyD88 in bEnd.3 cells after treatment (n = 6). (e) p-P65/P65 of NF-κB in bEnd.3 cells after treatment (n = 6). (f) TNF-α in bEnd.3 cells after treatment (n = 6). (g) IL-1β in bEnd.3 cells after treatment (n = 6). (h) IL-6 in bEnd.3 cells after treatment (n = 6). Statistical analysis was performed with one-way ANOVA followed by Dunnett-t test (*P < 0.05, **P < 0.01, ***P < 0.001).

LPS-promoting genera decreased, presumably further assisting in reducing inflammation in vessel endothelial cells [46–48].

In the present study, significant correlations of Gal-3 with δ-VB, SCFAs, and LPS (Figs. 8(a) and (b)) were demonstrated. Notably, δ-VB and LPS were further involved in the activation of the TLR-4/MyD88/NF-κB inflammatory pathway in high-glucose-induced bEnd.3 cells, whereas SCFAs exhibited an inhibitory effect on this pathway (Fig. 8(e)). We found that SA, SP, SB, and MCP all significantly inhibited the production of Gal-3, suggesting that SCFAs oppress Gal-3. This result was consistent with reports that dietary fiber in pectin (such as MCP) suppressed Gal-3 levels through the production of SCFAs in the gut microbiota [49]. Moreover, LPS has been found to play a synergistic role with Gal-3 in stroke patients, as Gal-3 is required for the full activation of TLR-4 by LPS [50]. The relationship between δ-VB and Gal-3 has not been previously reported. Here, we found that both LPS and δ-VB aggravated the activation of the TLR-4/MyD88/NF-κB inflammatory pathway in epithelial cells.

The biological relationships among host vessel endothelium, hyperglycemia, and intestinal bacteria could be complex. Effective treatment of DE requires comprehensive therapy, to both reduce blood glucose levels and protect cerebral vessels from inflammation. This study suggests that the gut microbiota is part of the solution and that BBR has potential as a drug for the treatment of DE. In the future, well-designed clinical studies are needed to draw conclusions regarding the use of BBR to treat DE.

CRediT authorship contribution statement

Zheng-Wei Zhang: Writing – original draft, Validation, Methodology, Investigation, Formal analysis, Data curation.

Wei-Ping Wang: Formal analysis, Data curation. **Jia-Chun Hu:** Methodology, Data curation. **Jin-Yue Lu:** Software, Methodology. **Ru Feng:** Resources, Methodology. **Shao-Feng Xu:** Methodology, Data curation. **Ling Wang:** Resources, Data curation. **Jie Fu:** Methodology. **Hang Yu:** Methodology. **Hui Xu:** Methodology. **Hao-Jian Zhang:** Methodology. **Xin-Yu Yang:** Methodology, Formal analysis. **Zhao Zhai:** Methodology, Formal analysis. **Jing-Yue Wang:** Methodology, Formal analysis. **Meng-Liang Ye:** Validation, Software, Investigation. **Heng-Tong Zuo:** Validation. **Jian-Ye Song:** Validation, Methodology. **Yi Zhao:** Validation, Methodology. **Xiang Hui:** Validation. **Xiao-Liang Wang:** Writing – review & editing, Supervision, Project administration, Methodology, Formal analysis. **Jian-Dong Jiang:** Writing – review & editing. **Yan Wang:** Writing – review & editing, Writing – original draft, Supervision, Project administration, Investigation, Funding acquisition, Conceptualization.

Declaration of competing interest

The authors declare that they have no known competing financial interests or personal relationships that could have appeared to influence the work reported in this paper.

Acknowledgments

The work was funded by the National Key Research and Development Program of China (2022YFA0806400), the CAMS Innovation Fund for Medical Sciences (CIFMS) (2023-I2M-2-006, 2021-1-I2M-027, and 2021-1-I2M-028), the National Natural Science Foundation of China (82173888 and 81973290), the Beijing Key Laboratory of Non-Clinical Drug Metabolism and PK/PD Study (Z141102004414062). We would like to thank Shimadzu (China) Co., Ltd. for the technological supports in this study.

Appendix A. Supplementary data

Supplementary data to this article can be found online at https://doi.org/10.1016/j.eng.2025.04.018.

References

[1] Gudala K, Bansal D, Schifano F, Bhansali A. Diabetes mellitus and risk of dementia: a meta-analysis of prospective observational studies. J Diabetes Investig 2013;4:640–50.
[2] Biessels GJ, Staekenborg S, Brunner E, Brayne C, Scheltens P. Risk of dementia in diabetes mellitus: a systematic review. Lancet Neurol 2006;5:64–74.
[3] Cukierman-Yaffe T, Gerstein HC, Williamson JD, Lazar RM, Lovato L, Miller ME, et al. for the Action to Control Cardiovascular Risk in Diabetes-Memory in Diabetes (ACCORD-MIND) Investigators. Relationship between baseline glycemic control and cognitive function in individuals with type 2 diabetes and other cardiovascular risk factors. Diabetes Care 2009;32:221–6.
[4] De Felice FG, Lourenco MV, Ferreira ST. How does brain insulin resistance develop in Alzheimer's disease? Alzheimers Dement 2014;10:S26–32.
[5] Nishikawa H, Suzuki H. Possible role of inflammation and galectin-3 in brain injury after subarachnoid hemorrhage. Brain Sci 2018;8:30.
[6] Soares LC, Al-Dalahmah O, Hillis J, Young CC, Asbed I, Sakaguchi M, et al. Novel galectin-3 roles in neurogenesis, inflammation and neurological diseases. Cells 2021;10:3047.
[7] Wątroba M, Grabowska AD, Szukiewicz D. Effects of diabetes mellitus-related dysglycemia on the functions of blood–brain barrier and the risk of dementia. Int J Mol Sci 2023;24:10069.
[8] Reis F. Soares, Nunes, Pereira, Diabetic encephalopathy: the role of oxidative stress and inflammation in type 2 diabetes. IJICMR 2012;2012:75–85.
[9] Mazumdar D, Singh S. Diabetic encephalopathy: role of oxidative and nitrosative factors in type 2 diabetes. Indian J Clin Biochem 2024;39:3–17.
[10] Zhou H, Zhang X, Lu J. Progress on diabetic cerebrovascular diseases. Bosn J Basic Med Sci 2014;14:185.
[11] Naufel MF, Truzzi GDM, Ferreira CM, Coelho FMS. The brain–gut–microbiota axis in the treatment of neurologic and psychiatric disorders. Arq Neuropsiquiatr 2023;81:670–84.
[12] Zhang ZW, Gao CS, Zhang H, Yang J, Wang YP, Pan LB, et al. Morinda officinalis oligosaccharides increase serotonin in the brain and ameliorate depression via promoting 5-hydroxytryptophan production in the gut microbiota. Acta Pharm Sin B 2022;12:3298–312.
[13] Zhao ZX, Fu J, Ma SR, Peng R, Yu JB, Cong L, et al. Gut–brain axis metabolic pathway regulates antidepressant efficacy of albiflorin. Theranostics 2018;8:5945–59.
[14] Yu JB, Zhao ZX, Peng R, Pan LB, Fu J, Ma SR, et al. Gut microbiota-based pharmacokinetics and the antidepressant mechanism of paeoniflorin. Front Pharmacol 2019;10:268.
[15] Zhang ZW, Han P, Fu J, Yu H, Xu H, Hu JC, et al. Gut microbiota-based metabolites of Xiaoyao Pills (a typical traditional Chinese medicine) ameliorate depression by inhibiting fatty acid amide hydrolase levels in brain. J Ethnopharmacol 2023;313:116555.
[16] Mossad O, Nent E, Woltemate S, Folschweiller S, Buescher JM, Schnepf D, et al. Microbiota-dependent increase in δ-valerobetaine alters neuronal function and is responsible for age-related cognitive decline. Nat Aging 2021;1:1127–36.
[17] Kong W, Wei J, Abidi P, Lin M, Inaba S, Li C, et al. Berberine is a novel cholesterol-lowering drug working through a unique mechanism distinct from statins. Nat Med 2004;10:1344–51.
[18] Yin J, Xing H, Ye J. Efficacy of berberine in patients with type 2 diabetes. Metabolism 2008;57:712–7.
[19] Zhang X, Zhao Y, Zhang M, Pang X, Xu J, Kang C, et al. Structural changes of gut microbiota during berberine-mediated prevention of obesity and insulin resistance in high-fat diet-fed rats. PLoS One 2012;7:e42529.
[20] Feng R, Shou JW, Zhao ZX, He CY, Ma C, Huang M, et al. Transforming berberine into its intestine-absorbable form by the gut microbiota. Sci Rep 2015;5:12155.
[21] Wang Y, Tong Q, Shou JW, Zhao ZX, Li XY, Zhang XF, et al. Gut microbiota-mediated personalized treatment of hyperlipidemia using berberine. Theranostics 2017;7:2443–51.
[22] Wang Y, Shou JW, Li XY, Zhao ZX, Fu J, He CY, et al. Berberine-induced bioactive metabolites of the gut microbiota improve energy metabolism. Metabolism 2017;70:72–84.
[23] Wang Y, Tong Q, Ma SR, Zhao ZX, Pan LB, Cong L, et al. Oral berberine improves brain dopa/dopamine levels to ameliorate Parkinson's disease by regulating gut microbiota. Signal Transduct Target Ther 2021;6:77.
[24] Ma SR, Tong Q, Lin Y, Pan LB, Fu J, Peng R, et al. Berberine treats atherosclerosis via a vitamine-like effect down-regulating choline–TMA–TMAO production pathway in gut microbiota. Signal Transduct Target Ther 2022;7:207.
[25] Pan L, Yu H, Fu J, Hu J, Xu H, Zhang Z, et al. Berberine ameliorates chronic kidney disease through inhibiting the production of gut-derived uremic toxins in the gut microbiota. Acta Pharm Sin B 2023;13:1537–53.
[26] Leger M, Quiedeville A, Bouet V, Haelewyn B, Boulouard M, Schumann-Bard P, et al. Object recognition test in mice. Nat Protoc 2013;8:2531–7.
[27] Shen Y, Hua L, Yeh CK, Shen L, Ying M, Zhang Z, et al. Ultrasound with microbubbles improves memory, ameliorates pathology and modulates hippocampal proteomic changes in a triple transgenic mouse model of Alzheimer's disease. Theranostics 2020;10:11794–819.
[28] Li A, Gong H, Zhang B, Wang Q, Yan C, Wu J, et al. Micro-optical sectioning tomography to obtain a high-resolution atlas of the mouse brain. Science 2010;330:1404–8.
[29] Nunez J. Morris water maze experiment. J Vis Exp 2008;19:897.
[30] Nakai K, Imai H, Kamei I, Itakura T, Komari N, Kimura H, et al. Microangioarchitecture of rat parietal cortex with special reference to vascular "sphincters". Scanning electron microscopic and dark field microscopic study. Stroke 1981;12:653–9.
[31] Corem N, Anzi S, Gelb S, Ben-Zvi A. Leptin receptor deficiency induces early, transient and hyperglycaemia-independent blood–brain barrier dysfunction. Sci Rep 2019;9:2884.
[32] Li X, Cai Y, Zhang Z, Zhou J. Glial and vascular cell regulation of the blood–brain barrier in diabetes. Diabetes Metab J 2022;46:222–38.
[33] Zhang X, Yin X, Zhang J, Li A, Gong H, Luo Q, et al. High-resolution mapping of brain vasculature and its impairment in the hippocampus of Alzheimer's disease mice. Natl Sci Rev 2019;6:1223–38.
[34] Kim SY, Buckwalter M, Soreq H, Vezzani A, Kaufer D. Blood–brain barrier dysfunction-induced inflammatory signaling in brain pathology and epileptogenesis: blood–brain barrier dysfunction. Epilepsia 2012;53:37–44.
[35] Takata F, Nakagawa S, Matsumoto J, Dohgu S. Blood–brain barrier dysfunction amplifies the development of neuroinflammation: understanding of cellular events in brain microvascular endothelial cells for prevention and treatment of BBB dysfunction. Front Cell Neurosci 2021;15:661838.
[36] Li P, Liu S, Lu M, Bandyopadhyay G, Oh D, Imamura T, et al. Hematopoietic-derived galectin-3 causes cellular and systemic insulin resistance. Cell 2016;167:973–84.
[37] Ma J, Feng R, Tan X, Ma C, Shou J, Fu J, et al. Excretion of berberine and its metabolites in oral administration in rats. J Pharm Sci 2013;102:4181–92.
[38] Walker AW, Duncan SH, McWilliam Leitch EC, Child MW, Flint HJ. pH and peptide supply can radically alter bacterial populations and short-chain fatty acid ratios within microbial communities from the human colon. Appl Environ Microbiol 2005;71:3692–700.
[39] Feng W, Ao H, Peng C. Gut microbiota, short-chain fatty acids, and herbal medicines. Front Pharmacol 2018;9:1354.
[40] Scales BS, Dickson RP, Huffnagle GB. A tale of two sites: how inflammation can reshape the microbiomes of the gut and lungs. J Leukoc Biol 2016;100:943–50.
[41] Engelmann C, Sheikh M, Sharma S, Kondo T, Loeffler-Wirth H, Zheng YB, et al. Toll-like receptor 4 is a therapeutic target for prevention and treatment of liver failure. J Hepatol 2020;73:102–12.

[42] Tuttle KR. Linking metabolism and immunology: diabetic nephropathy is an inflammatory disease. J Am Soc Nephrol 2005;16:1537–8.
[43] Zhou W, Ke S, Li W, Yuan J, Li X, Jin R, et al. Mapping the function of whole-brain projection at the single neuron level. Adv Sci 2022;9:2202553.
[44] Zhao M, Wei H, Li C, Zhan R, Liu C, Gao J, et al. Gut microbiota production of trimethyl-5-aminovaleric acid reduces fatty acid oxidation and accelerates cardiac hypertrophy. Nat Commun 2022;13:1757.
[45] Zhang ZW, Cong L, Peng R, Han P, Ma SR, Pan LB, et al. Transformation of berberine to its demethylated metabolites by the CYP51 enzyme in the gut microbiota. J Pharm Anal 2021;11:628–37.
[46] Morrison DJ, Preston T. Formation of short chain fatty acids by the gut microbiota and their impact on human metabolism. Gut Microbes 2016;7:189–200.
[47] Diks S, Richel D, Peppelenbosch M. LPS signal transduction: the picture is becoming more complex. Curr Top Med Chem 2004;4:1115–26.
[48] Li Z, Geng YN, Jiang JD, Kong WJ. Antioxidant and anti-inflammatory activities of berberine in the treatment of diabetes mellitus. Evid Based Compl Alt 2014;2014:1–12.
[49] Pedrosa LF, Raz A, Fabi JP. The complex biological effects of pectin: galectin-3 targeting as potential human health improvement? Biomolecules 2022;12:289.
[50] Burguillos MA, Svensson M, Schulte T, Boza-Serrano A, Garcia-Quintanilla A, Kavanagh E, et al. Microglia-secreted galectin-3 acts as a Toll-like receptor 4 ligand and contributes to microglial activation. Cell Rep 2015;10:1626–38.